Geochemical characteristics of rare earth elements in sediments of the North China Plain: implication for sedimentation process

Haiyan Liu, Huaming Guo, Olivier Pourret, Maohan Liu

Geochemical characteristics of rare earth elements in sediments of the North China Plain: implication for sedimentation process

Haiyan Liu [1,*], Huaming Guo [2], Olivier Pourret[3], Maohan, Liu[1]

[1] *School of Water Resources and Environmental Engineering, East China University of Technology, Nanchang 330013, P. R. China*

[2] *School of Water Resources and Environment, China University of Geosciences (Beijing), Beijing 100083, P.R. China*

[3] *UniLaSalle, AGHYLE, Beauvais, France*

*** Corresponding author:** Haiyan Liu

No. 418 Guanglan Road, Jingkai District, Nanchang 330013, P. R. China

E-mail address: hy_liu@ecut.edu.cn

Tel.: +86-1881-3181-419

Fax: +86-0791-8389-8197

H. Guo: No. 29 Xueyuan Road, Haidian District, Beijing, P. R. China

O. Pourret: 19 rue Pierre Waguet-BP 30313, 60026 Beauvais, France

M. Liu: No. 418 Guanglan Road, Jingkai District, Nanchang 330013, P. R. China

Abstract: Rare earth elements (REE) are powerful tracers for our understanding of sedimentary provenance and depositional processes. The present study investigated geochemical characteristics of REE in 226 sediment samples collected from piedmont, central and littoral plains of the North China Plain. Results showed that average total REE concentrations exhibited a decreasing trend as piedmont > central > littoral, and 82%, 70% and 67% samples had total REE concentrations higher than the value of Upper Continental Crust (UCC). The variation in REE concentrations was associated with sedimentary provenance and sediment physicochemical properties. Ternary diagrams of sandstone classification and Al_2O_3-CaO+Na_2O-K_2O reflected that sediments originated from greywackes and they have been experienced an incipient to intermediate chemical weathering with piedmont sediments to a higher degree. Average Chemical Index of Alteration values are 68, 51 and 55 in piedmont, central and littoral sediments, respectively. Sediment North American Shale Composite (NASC)-normalized patterns were characterized by light REE (LREE) enrichment over heavy REE (HREE) and coherent negative Eu anomalies (Eu/Eu* ranging between 0.57 and 1.00). Value of $(La/Yb)_{NASC}$ ranged from 0.86 to 1.15 (average 1.23), and from 1.03 to 1.49, and from 0.91 to 1.49 in three zones, indicating REE fractionation from piedmont to littoral occurred over sedimentation processes. A positive correlation between $(La/Yb)_{NASC}$ and total REE concentrations was observed in piedmont and central sediment samples, implying that LREE were preferentially enriched over HREE with an accumulation of REE. While this correlation was not found in littoral sediment samples, where a general decreasing trend along depth for

REE concentrations existed. Results of present study shows implications for using REE as a tracer of sedimentary provenance from a basin scale.

Keywords: Lanthanides; Geochemistry; Sedimentation; Fractionation; Critical Zone

1. Introduction

Rare earth elements are the lanthnides with atomic numbers ranging from 57 (La, lanthanum) to 71 (Lu, lutetium) (Henderson, 1984) as well as yttrium (Y, atomic number 39) and scandium (Sc, atomic number 21; Tyler, 2004). The geochemical signatures of rare earth elements and yttrium (thereafter denoted REE) in sediments and sedimentary rocks are powerful tracers in delineating the processes that govern them. These include magmatism, chemical weathering, diagenesis, erosion and water-rock interactions (McLennan, 1989). As a result, the concentrations and fractionations of REE in sediments and soils have received considerable attention in the past few decades.

Numerous investigations have been devoted to studying geochemical behaviors and mobility of REE in different sediments and soils, including lake, river and marine sediments (Pourret and Tuduri, 2017; Xu et al., 2018, Wang et al., 2018; Consani et al., 2020), mining surroundings (Hu et al., 2004; Wang and Liang, 2015), wetlands (Davranche et al., 2011; Cheng et al., 2012), agricultural areas (Silva et al., 2015; Han et al., 2017), alluvial deposits (Pédrot et al., 2015; Xie et al., 2014), unconsolidated clay sediments (Guo et al., 2010; Sá Paye et al., 2016) and sedimentary rocks (McLennan, 2001; Šmuc et al., 2012). It's recognized that REE concentrations and distributions in sediments depend on sedimentary provenance and sediment's physicochemical properties. Significant correlations between REE concentrations and contents of clay and metals (i.e., Fe, Mn, Al) were observed by Mihajlovic and Rinklebe (2018); while pH value and cation exchange capacity were shown not

important factors in their study. Grain size impacted REE concentrations in sediment as well. This is indicated by the results of Kimoto et al. (2006), showing that decreasing grain size generally increased REE concentrations due to that clay minerals could host REE (Laveuf and Cornu, 2009). More specific, the impact of clay, silty and sand fractions on solid REE was recently investigated in different soil profiles (Mihajlovic and Rinklebe, 2018). Presence of Fe/Mn oxides was another factor influencing REE in sediments/soils, and more REE can be accumulated by amorphous Fe/Mn oxides as compared to crystalline ones (Yan et al., 1999; Compton et al., 2003).

Constituents of REE in sediments and soils for a large part result from natural processes. A global distribution pattern of REE in the soils/sediments was recently evaluated by Adeel et al. (2019), which was achieved by spatially visualized the distribution of the REE concentrations in soils/sediments derived from all over the world. Results obtained from the study showed that total REE concentrations of agriculture soils/sediments ranged from 83 to 9840 mg/kg and concentrations of light REE (LREE) were higher than heavy REE (HREE). This indicates that, in addition to the natural processes, anthropogenic inputs contribute to the REE concentrations in sediments/soils in some individual regions. Indeed, fertilization with REE-bearing fertilizers and infiltration of residuals was suggested to be the main mechanism of agriculture-sourced REE entering into soils and sediments (Hu et al., 2004). However, mechanisms for REE mobilization in different soils/sediments and the potential risks of long-term exposure to REE-abundant environment are not adequately understood.

Average REE concentration in China's soil was established to be 177 mg/kg (Liang et al., 2005), being comparable to the value (189 mg/kg) in the earth's crust (Wei et al. 1991). China is one of the countries that early widely applied REE in various sectors (Pang et al., 2002; Hu et al., 2006), such as agriculture, the REE have been used as a prompter for crops since 1990s. This has led to high REE pollution levels (i.e. La >80; Nd >85; Sm >45) (Adeel et al., 2019; and references therein). Indeed, sediment and soil contaminations caused by elevated REE have been reported in various regions across China, including in Poyang lake (Wang et al., 2018), Baotou city (Li et al., 2010), Tibet plateau (Wu et al., 2018), Jiaozuo Bay (Zhang and Gao, 2015), Sanjiang Plain (Cheng et al., 2012) and Liaodong Bay (Lin et al., 2013). The North China Plain (NCP) is one of the largest sedimentary basin in Asia (Xing et al., 2013), and is provincial politics, economy and culture center of China. The plain is characterized by large population (> 0.35 billion) and highly-developed agricultural industry, which plays an important role in the nation's grain manufacture (Chen and Ni, 1987; Kendy et al., 2004). The densely-populated and industrialized areas were shown to be accompanied by increased discharge of REE into environment (i.e., Gd and Sm) (Kulaksız and Bau, 2013; Hatje et al., 2016), due to REE applications in industry, medicine as well as agriculture. Studies concerning REE concentrations in sediments of the NCP have been performed (Wei et al., 2010; Liu et al., 2016; Zhang and Gao, 2015; Liu et al., 2019a, b), but a full of investigation of mobility, distributions and behaviors of REE in sediments is still lacking. This would hinder a systematical evaluation of REE levels as well as the possible anthropogenic impact,

which is vital for establishing a baseline of distribution and background of REE concentration in the contaminated sediments and for administrating regulation guidelines (Alfaro et al., 2018; Consani et al., 2020). Therefore, the objectives of this study are to: (i) investigate REE concentration and fractionation characteristics in sediments collected from three zones; (ii) characterize the relationships between REE distribution and sediment properties; (iii) provide dataset concerning REE geochemistry for future comparative studies in the region.

2. Material and methods

2.1 Study area

The North China Plain (NCP) is located in the eastern China with longitude of 112°30'~119°30'E, and latitude of 34°46'~40°25'N. The terrains are mostly plains with two mountainous regions (Yanshan and Tanghang mountains) bounding to the north and south, and an oceanic region (Bohai Bay) to the east (Chen et al., 1999), respectively. The plain has a total area of approximately 31×10^4 km^2 and population of about 0.35 billion inhabitants. The NCP has a semi-arid humid climate with a temperature range of -23 °C~42.7 °C (in history). Average annual rainfall ranges from 500 mm to 600 mm, mostly (>74%) dominating in summer. Average annual evaporation is 1.5 to 3 times of annual rainfall.

The NCP is one of largest sedimentary basins in Asia (Xing et al., 2013). According to Chen et al. (1999), the NCP's geological strata are comprised of four stratigraphic areas: Yinshan-Nuruerhu, Yanshan, Taihangshan and Hebei, with ages

ranging from the oldest Archaeozoic to the newest Holocene. Formations in study area have been declining since the Cenozoic due to neotectonics. Geographically, the plain generally decreases from the north to the east with a slope of 0.3‰~0.6‰, and thus it's divided into three zones: piedmont alluvial-proluvial plain, central alluvial-lacustrine plain and littoral plain.

Surface sediments in the NCP mainly are Cenozoic deposits with ages from Paleogene to Holocene. Lower Tertiary stratum is composed of red mudstone with red and gay sandstone being interbeded. Upper Tertiary strata are characterized by consolidated to semi-consolidated alluvial-diluvial deposits, including siltstone, mudstone, sandstone and pebbly sandstone. Quaternary sediments are divided into four groups from top to bottom: Holocene (Q4), Upper (Q_3m), Middle (Q_2c) and Lower (Q_1n) Pleistocene (Chen, 1999). The Holocene sediments group has a thickness of 5 m to 40 m, and mainly consists of yellow and gray sandy loam, fine sand and clay being interbedded with sandy gravel. The Upper Pleistocene is alluvial, diluvial and eolian losses and yellow loam. The Middle Pleistocene stratums are widely distributed in intermountain basin and foothills, and consist of red and brown clay, loam and sandy loam, and red mud pebble layers. The Lower Pleistocene sediments group has a buried depth of 350 m to 500 m with a thickness of 80 m to 100m, and it's mainly loam, sand loam and lenticular sand layers.

Piedmont alluvial-proluvial sediments are suggested to derive from Taihang and Yanshan mountains by weathering, transport and sedimentation process. Central alluvial-lacustrine sediments are deposited from materials carried by Yellow River

and Zhangweinan River running from SW to NE since middle Pleistocene (Shao et al., 1989). The littoral plain forms with interactions between terrene and ocean, and sedimentary deposits come from terrestrial rivers draining into Bohai Bay eventually.

2.2 Sediment sampling

Sediment samples were taken from three boreholes (Y09, S30 and H02) drilled in three different zones (Fig. 1) of the NCP in the July of 2013. The core sediments were sampled with an interval generally ranging between 1 m and 2 m. Slurries and muds attached on the surface of the core sediments were scrapped off to avoid possible cross contaminations. The samples were parceled with silver paper and were stored in clean plastic bags which were immediately filled with pure N_2 gas for further preservation. All the sealed core sediments were placed in a shading environment with temperature below 4 °C during sampling. Finally, the samples were transported to laboratory and preserved in a freezer before analysis.

2.3 Sediment analysis

All samples used for major and minor constituents analyses were dried under room temperature in the lab, and were ground to grain size <74 μm with an agate mortar for analysis. The X-ray fluorescence (XRF) (ARL Advant X) technique was used for measurement of various oxides (SiO_2, Fe_2O_3, Al_2O_3, MgO, CaO, Na_2O, K_2O, MnO, P_2O_5 and TiO_2) following the national standard method (GB/T 14506). Sediment samples were prepared with a glass flux sheet method. Specifically, 0.7 g ($\pm$0.001) sample was firstly placed in a 25 mL porcelain crucible; followed by

addition of 5.2 g (±0.001) anhydrous lithium tetraborate, 0.4 g (±0.001) lithium fluoride and 0.3 g (±0.01) ammonium nitrate, the mixture was evenly stirred. Then the mixture was transferred to a platinum (95%)-gold (5%) alloyed crucible for fusing 10 to15 mins under temperature 1150 to 1250 ℃. Finally, fusant was made into glass beads using a fusion machine. All glass beads were preserved in a clean and dry environment before analysis. Reference materials GSS (shown below) were prepared with the same method for subsequent calibration of XRF. The sample intensity (I_S) was calculated by the difference between peak (I_p) and background (I_b) values, as shown with equation (2-1).

$$I_S = I_p - I_b \quad (2\text{-}1)$$

Trace elements including REE were quantified by employing ICP-MS (AG 7500) in the digested samples. The samples were digested following the method previously described in Liu et al. (2016). Briefly, 9 mL concentrated HCl (37% v/v), 2 mL HNO_3 (65% v/v) and 9 mL HF (40% v/v) were used for digesting 0.5 g dried samples for 24 h under 108 °C condition. Then the mixture was dried and dissolved again with purified HNO_3 (2% v/v). The obtained solutions were used for trace element analysis. To check the stability of the equipment system and the analytical accuracy, reference sample including GSS1, GSS2, GSS3 and GSS5, obtained from the Center of China National Standard Reference Material, were ran simultaneously. The recommended and test values of REE and metal oxides in standard references were shown in supplementary materials (Table S1). Furthermore, the parallel sample was performed every ten samples for further monitoring of the analytical precisions. The results show

200 that elements mostly had accuracies (RSD, δ1) ranging between 2% and 5%. The
201 standard materials had accuracy generally better than 3%, except for P_2O_5, which had
202 an accuracy better than 8% in some samples. The analytical precisions of REE in all
203 samples were generally better than 5%.

204 2.4 REE normalization

205 Rare earth element concentrations in all sediment samples were normalized with
206 average REE concentrations of the North American Shale Composite (NASC). The
207 corresponding normalization REE values were taken from Taylor and McLennan
208 (1985). Fractionation between LREE and HREE was quantified using fractionation
209 measures [$(La/Lu)_{NASC}$ and $(Nd/Yb)_{NASC}$)]. Anomalies including Ce (Ce/Ce*) and Eu
210 (Eu/Eu*) were calculated by extrapolation using normalized values of neighboring
211 REE. The corresponding formulas were shown with equations (2-2) to (2-4).

$$Ce/Ce^* = Ce_{NASC}/(La_{NASC} \times Pr_{NASC})^{0.5} \quad (2\text{-}2)$$

$$Eu/Eu^* = Eu_{NASC}/(Sm_{NASC} \times Gd_{NASC})^{0.5} \quad (2\text{-}3)$$

$$Gd/Gd^* = Gd_{NASC}/(Eu_{NASC} \times Tb_{NASC})^{0.5} \quad (2\text{-}4)$$

212 where the superscript * indicates the geogenic background.

213

214 **3. Results and discussion**

215 3.1 Sediment geochemistry and provenance

216 Sediment lithology in three boreholes are mainly clay, silt and silty clay (Fig. 2).
217 Fine and course sands were generally interbedded with silt and silty clay at different

sampling depths. This is better observed in the central (S30) and littoral (H02) borehole bar graphs (Figs. 2b and c). In piedmont borehole, a gravel layer occurred at depth between 38 m and 61 m (Fig. 2a). Gravel was not found in boreholes S30 and HH02. Overall, fine grains prevailed in central and littoral sediment samples. Colors of the fine grains changed in three zones as well. Pale yellow and pale brownish-yellow clay and silty were mainly distributed in piedmont sediments. For central borehole sediments, the color changed from pale brownish-yellow to brown and tan vertically. For littoral sediments, taupe and tawny silty and silty clay were mainly in upper and middle parts, and pale brownish-yellow and pale brown in lower part (Fig. 2c).

The component of sediment samples was dominated by SiO_2 (Table 1). For piedmont sediments (borehole Y09), contents (wt%) of SiO_2 ranged from 55.55 to 78.36 with an average value of 66.77. Central (borehole S30) and littoral (borehole HH02) sediments had SiO_2 contents (wt%) lower than those of piedmont, being in the ranges of 35.71 to 71.56 (average 56.62) and 32.04 to 77.03 (average 59.51), respectively. Aluminum oxide (Al_2O_3) had the highest contents among the determined metal oxides, with ranges of 6.37 wt% to 14.14 wt%, 7.42 wt% to 13.82 wt% and 7.32 wt% to 15.95 wt% and average values of 10.47 wt%, 10.95 wt% and 12.18 wt% in piedmont, central and littoral sediments, respectively. Iron oxide (Fe_2O_3) was the second abundant metal oxides, with a range from 1.86 wt% to 9.86 wt% and an average of 5.46 wt% in piedmont sediments. The average content (wt%) of Fe_2O_3 in central and littoral sediments was 4.45 wt% and 4.06 wt%, respectively, exhibiting

slightly lower than that of piedmont sediments. Other metal oxides including Na_2O, K_2O, CaO, MgO, P_2O_5 and TiO_2 showed relatively lower content in most of the measured sediment samples as compared to SiO_2 and Al_2O_3 (Table 1). Average value (wt%) of loss on ignition (LOI) was 3.88, 8.56 and 8.02 in piedmont, central and littoral zones with ranges of 1.13 to7.36, 3.12 to 19.91 and 2.5 to 17.56, respectively.

Changes of sediment lithology were related to the sedimentary provenances and processes (McLennan, 2001). Piedmont sediments were thought to be derived from piedmont regions (Taihang and Yanshan Mountains), where coarse-grained clastic rocks were widely distributed (Zhang et al., 2018). Occurrences of central sediments were attributed to fluviation of Yellow river and rivers springing in Taihang Mountain (Zhang et al., 2018). This would account for sediments being deposited alternately with clay, silty clay and fine sand (Fig. 2). Terrigenous clastics deposition and the impact of ocean led to the formation of littoral sedimentation. Weathering and erosion of the bedrocks around the piedmont plain and subsequent transport and sedimentation contributed to the NCP sediments. Ternary diagram of sandstone classification (Blatt et al., 1980) showed that the majority of sediment samples were located in the left area, and three central samples in the right area, indicating that sediments originally mostly were greywacke (Fig. 3a). The dominant SiO_2 contents and fine-grained components reflected that the sedimentary materials had been undergone intensive denudations and a long-distance transport before sink. Indeed, the ternary diagram of Al_2O_3-CaO+Na_2O-K_2O (A-CN-K) showed that the weathering trend of the sediment samples were mostly along the axis of (CaO+Na_2O) (Fig. 3b).

This probably indicates that sediment samples from the NCP were in an early weathering stage where minerals such as plagioclase was incongruently decomposed in association with leaching of Na and Ca generating products of illite, kaolinite and smectite (Nesbitt et al., 1980). The offset to the uppermost of K_2O axis was attributed to the addition of terrigenous detrital in the later sedimentary stage (Cox et a1., 1995).

To quantify the weathering intensity in different samples, the chemical index of alteration (CIA) values (initially was valid for granitic rocks) were calculated following the method proposed by Nesbitt and Young (1982) [CIA = $(Al_2O_3/(Al_2O_3 + K_2O + Na_2O + CaO^*))\times100$; $CaO^* = [CaO - (10/3\times P_2O_5)]$ (Panahi et al., 2000)]. Chemical index of alteration can be an index reflecting sample in a weathering trend from fresh status to intensely-altered status. Granites and granodiorites usually have CIA values ranging from 45 to 50, and fresh basalts have values between 30 and 45. Muscovite has a value of 75, and illite, montmorillonites and beidellites give values from 75 to 85 (Nesbitt and Young, 1982). Results showed that CIA value of piedmont sediment samples ranged from 55 to 78 with an average value of 68, and central and littoral samples ranged from 37 to 70 (average 51), and from 43 to 70 (average 55), respectively. This indicates that sediment samples were incipiently (CIA: 50 to 60) to intermediately (CIA: 60 to 80) chemically weathered, according to the classification standards suggested by Fedo et al. (1995). It’s also observed that piedmont sediment samples generally had higher CIA values as compared to those of central and littoral sediments, which means a stronger weathering may have occurred in the piedmont sediment samples. These differences probably were associated with the

hydrogeological conditions (i.e. groundwater residence time, outcrop lithology and aquifer replenishment condition). The results were consistent with piedmont samples being located in the upper part of the A-CN-K diagram, while central and littoral sediment samples below the piedmont samples (Fig. 3b). Similar studies have been performed to investigate the impact of chemical weathering on sedimentary processes based on sediment geochemical compositions (LaMaskin et a1., 2008; Dostal and Keppie, 2009; Xie et al., 2014). Conclusions have been made that sediment geochemistry could serve as a good proxy for understanding the origins and processes of sedimentation, as shown in the investigation.

3.2 REE distribution characteristics

3.2.1 REE concentrations

Total REE (ΣREE) concentrations were shown in Table 1. Piedmont sediment (borehole Y09) ΣREE ranged from 190 mg/kg to 354 mg/kg with an average value of 227 mg/kg. Sediments from central (borehole S30) and littoral (borehole H02) zones had ΣREE concentrations ranging from 89 mg/kg to 291 mg/kg (average 183mg/kg) and from 87.90 mg/kg to 238 mg/kg (average 177 mg/kg), respectively. Generally, sediment ΣREE concentrations showed a decreasing trend (piedmont > central > littoral) along groundwater flow direction. The average ΣREE concentrations in littoral sediment samples from study area were comparable to the values of Upper Continental Crust (UCC) (169 mg/kg) (McLennan, 2001) and Chinese soil (177 mg/kg) (Wei et al., 1991). While average ΣREE concentrations of littoral and central

sediments were higher than the values of UCC and soil in China. All measured average REE concentrations were within in the levels (166 mg/kg to 222 mg/kg) reported in similar researches performed in the same study area (Lan et al., 2016). Others showed that core sediments' ΣREE concentrations were slightly higher than the value of surface sediment (Liu et al., 2019b).

Sediment ΣREE concentrations varied along depth. In piedmont borehole, ΣREE were relatively constant within 11 m below sea level. A small decrease was observed at depth from 11 m to 16 m, before ΣREE concentrations increased to >300 mg/kg at 25 m. After a new decrease until about 63 m, ΣREE concentrations fluctuated for the remaining sampling depths (Fig. 2a). ΣREE concentrations in central sediments were highly variable along borehole, although a decreasing trend occurred from land surface to 30 m. Vertical changes of ΣREE concentrations were mainly related to sediment physicochemical properties. Sediment with different grain sizes, such as clay, silt and silty clay, had different capacities in hosting REE. The major minerals in the aquifer sediments of study area included quartz, K-feldspar, hornblende and calcite accounting for 5%-14% in the piedmont (Chen and Ni, 1987). Clay minerals (i.e. kaolinite, illite and montmorillonite) were more commonly distributed in the central and littoral plains as compared to the piedmont plain (Chen et al., 2005). In piedmont where fine sand prevailed (i.e. from 38 m to 62 m), ΣREE concentrations progressively decreased (Fig. 2a). Low ΣREE concentrations of central sediments were found at depth of approximately 30 m, 65 m to 68 m, 107 m, 151 m to 154 m, where fine sands were sandwiched with silt and silty clay (Fig. 2b). Silt sand and fine

sand more commonly occurred at deeper depth, leading to a decreasing trend of ΣREE concentrations (Fig. 2c). This demonstrates that presence of clay was one of factors controlling ΣREE concentrations. REE were thought to be hosted by clay component containing in the sediments (Yang et al., 2002). The disparities of clay content along depth for a large part could account for REE variations. This was further supported by the vertical variations of Si/Al and Ti/Al values, which were proxies for grain size classification (i.e. clay, silt, and silty clay) (Fig. S2). Statistical analyses showed that ΣREE concentrations were negatively correlated to SiO_2 and were significantly positively correlated to Fe_2O_3 and Al_2O_3 (except for littoral sediment samples) (Table 2), reflecting that REE mainly adsorbed onto/incorporated into Fe and Al -containing oxides/clay minerals while repelled SiO_2. Moreover, trends of SiO_2/Al_2O_3 values were generally consistent with those of CIA, suggesting that silicate weathering like feldspar played a role in this process (Fig. 2). In other words, in addition to clay content, Fe and Al-bearing oxides could be another factor influencing REE concentrations in investigated sediment samples. Metal oxides containing Fe, Mn and Al provides important binding sites for sorption of REE (Ohta and Kawabe, 2000; Pourret and Davranche, 2013; Liu et al., 2017; Mihajlovic et al., 2019). These findings are in line with the results documented by Wang et al. (2014), showing that fine fractions with abundant clay minerals and Fe/Al/Mn-containing oxides tended to accumulate REE, while coarse fractions with less clay minerals and more quartz led to a dilution of REE. However, further information on mineralogical compositions of sediment samples is needed for better cons training the impact of mineralogy on REE

concentrations from a quantitative perspective. In all, sediment REE concentrations were essentially regulated by their genetic properties and were revealed by their vertical variations.

3.2.2 REE fractionation patterns

All sediment samples had relatively flat NASC-normalized REE patterns with a gentle enrichment of LREE over HREE (Fig. 4). The degree of LREE enrichment was quantified by $(La/Yb)_{NASC}$ values, which ranged between 0.86 and 1.15 with an average of 1.23 in piedmont sediments. Central and littoral sediment samples had $(La/Yb)_{NASC}$ ranges of 1.03 to 1.14 (average 1.21) and 0.91 to 1.49 (average 1.09), respectively (Table 1). Sediments mostly showed negative Ce anomalies with Ce/Ce* ranging between 0.69 and 1.17 (average 0.91), and between 0.85 and 0.98 (average 0.90), and between 0.80 and 0.98 (average 0.89) in piedmont, central and littoral plains, respectively. Negative Eu anomalies commonly occurred in investigated sediments with Eu/Eu* ranges of 0.82 to 1.07 (average 0.91), 0.83 to 1.31 (average 0.95), and 0.86 to 1.34 (average 0.95) in three zones, respectively. Correlation analysis indicated that ΣREE concentrations generally increased with an increase of $(La/Yb)_{NASC}$ in piedmont and central sediments, while this trend was not observed in littoral sediment samples (Fig. 5a). These results reflected REE fractionation occurred with the accumulation processes. The correlation between $(La/Yb)_{NASC}$ and CIA values showed that the larger $(La/Yb)_{NASC}$ values occurred in samples containing higher REE concentrations and generally having higher CIA values (Fig. 5b). Thus, LREE enrichment could result from the chemical weathering of silicate in crustal

materials leading to an increase in LREE concentrations in sediments (Oliveira et al., 2003; Lin et al., 2013). Larger CIA values were obtained in piedmont and central zones as compared to the values in littoral zones (discussed above). The different domain of littoral sediment samples from their piedmont and central counterparts may be related to impact of ocean and/or human activities as well. However, more studies are needed to verify this speculation.

Sediment samples mostly had negative Eu anomalies (Fig. 5d). Average Eu/Eu* anomalies were quite similar in three different zones. This indicated that sedimentary processes, which evolved weathering of bedrocks around plains and migration and deposition in the flat plains, did not fractionate Eu to a larger extend with respect to its neighboring Sm and Gd. Early investigations demonstrated that Eu compositions and distributions in continental crust were fundamentally controlled by shallow, intracrustal differentiation evolving Eu-bearing minerals (i.e. plagioclase) (McLennan, 2001), which was shown to possess 4% to 23% (wt) in piedmont sediments (Liu et al., 2016). However, Eu/Eu* values were negatively correlated to ΣREE concentrations (Fig. 5d), which suggested that evolution of Eu anomalies was related to changes of redox conditions as well during sedimentation. Preferential mobilization of Eu(II) over other trivalent REE leads to a segregation of Eu from lanthanide series under reducing conditions (Lee et al., 2003), and hence higher ΣREE concentrations occur in lower-Eu/Eu* samples, as shown in Figure 5d. This mechanism has been proposed for using Eu anomalies as an indicator for investigating REE origins as well as mobility of redox-sensitive metal(oid) (Guo et al., 2010; Davranche et al., 2011).

393 Another possibility resulting in negative correlation between Eu anomalies and ΣREE
394 concentrations would be related to minerals contained in sediments. Such as
395 plagioclase, which tends to preferentially accumulate Eu(II) over trivalent REE by
396 means of isomorphism with Ca^{2+}, Na^{+} and K^{+} (Banks et al., 1999).

397 Cerium anomalies (Ce/Ce*) were relatively constant in central and littoral
398 sediments despite the variable ΣREE concentrations, while they were distributed
399 scattered as a function of ΣREE concentrations in piedmont sediment samples (Fig.
400 5c). The fluctuation of redox conditions could account for this phenomenon due to
401 fact that Ce is readily to be precipitated as insoluble Ce(IV) via oxidative scavenging,
402 and when conditions evolve into reducing, the precipitated Ce will be released into
403 solution by reductive dissolutions (Bau and Koschinsky, 2009; Steinmann and Stille,
404 2008). Cerium cycle was believed to be biologically mediated (Moffett, 1990; Tanaka
405 et al., 2010) and evolved metal (i.e. Fe, Mn) oxides (Yu et al., 2017). Results of our
406 recent study showed that Ce precipitation from oxic aqueous solution was more likely
407 to occur in the piedmont aquifers where low-Fe/Mn-concentration groundwater
408 prevailed (Liu et al., 2019a), while no pronounced positive Ce anomalies were
409 commonly observed in the piedmont aquifer sediments. Thus, both positive and
410 negative Ce anomalies, and no Ce anomalies can be found in solid phases in nature, as
411 the results shown in present study.

412 3.3 Implication for REE signatures

413 Statistical analyses showed that individual REE concentrations were significantly
414 correlated with correlation coefficient (R^2) all better than 0.8. These results, together

with the findings that all investigated sediment samples had coherent normalized patterns, indicated that sediments had similar sources/inputs of REE as well as common geochemistry. The remarkable uniformity of sedimentary REE patterns, with absolute concentration ranging from La to Lu, slight LREE enrichment and common negative Eu anomalies, implied that REE were migrated and transported as an integral whole during chemical weathering and sedimentation processes including erosion, sedimentary sorting and diagenesis. The sediment paralleled NASC-normalized REE patterns suggested that REE information recorded in sediments could serve as an ideal tool for studying crustal evolution and sedimentary provenance. The higher REE abundances in sediment than the values of UCC reflected that an enrichment of REE occurred during the process of sedimentation. Since sedimentary REE uniformity was thought to result from effective mixing of various provenance components from the upper crust (McLennan, 2001) and they were transported primarily in particulates, the sedimentary origins and secondary mobilization would be the plausible cause for higher REE abundance. It should be noted that, in addition to natural processes, REE can be accumulated in sediments and soils by various ways including sewage discharges (Verplanck et al., 2005; Hatje et al., 2016), agricultural activities (Alfaro et al., 2018) and atmospheric depositions (Tyler, 2004). Positive REE anomalies will show up in REE normalized patterns when individual elemental concentration is greater than its background value, as for Gd anomalies that have been reported worldwide (Ebrahimi and Barbieri, 2019). However, the sediments cannot suffer from anthropogenic pollutions in this study since no pronounced positive REE anomalies

were observed in their normalized patterns. In summary, sedimentary REE patterns conveys important information regarding the composition of the continental crust and anthropogenic impact.

4. Conclusions

226 sediment samples were collected from three different zones (i.e. piedmont, central and littoral) of the north China plain (NCP) to investigate the concentrations and fractionations of rare earth element (REE). Sediment geochemistry indicated that sediments mostly were derived from greywacke, as suggested by triangular diagram of sandstone classification. All sediment samples had been undergone incipient to intermediate weathering with average CIA of 68, 51 and 55 in three zones, respectively. Total REE concentrations ranged from 190.24 to 353.87 mg/kg (average 228.62 mg/kg), and from 88.85 to 290.80 mg/kg (average 182.88 mg/kg), and from 87.90 to 237.61 mg/kg (average 176.69 mg/kg) in piedmont, central and littoral plains, exhibiting a decreasing trend as piedmont > central > littoral. Sediment physicochemical properties such as mineral composites and metal oxide abundance controlled REE concentrations, as observed along depth in three sediment sampling profiles. All sediment samples had coherent NASC-normalized REE patterns that were characterized by light REE (LREE) enrichment over heavy REE (HREE) with $(La/Yb)_{NASC}$ ranging between 0.86 and 1.49. Negative Ce and Eu anomalies generally occurred in the investigated sediments with Ce/Ce* and Eu/Eu* ranges of 0.69 to 1.17 and 0.82 to 1.34, respectively. The present study provides important dataset for future studies in this region.

Acknowledgments

This investigation has been funded by National Natural Science Foundation of China (Nos. 41902243, 41222020 and 41172224), the program of China Geology Survey (No. 12120113103700), and the Fok Ying-Tung Education Foundation, China (Grant No. 131017). East China University of Technology Research Foundation for Advanced Talents (Nos. DHBK2019094 and SHT201901).

References

Adeel, M., Lee, J. Y., Zain, M., Rizwan, M., Nawab, A., Ahmad, M. A., Shafiq, M., Yi, H., Jilani, G., Javed, R., Horton, R., Rui, Y. K., C. W. Tsangk, D. and Xing, B. S., (2019) Cryptic footprints of rare earth elements on natural resources and living organisms. Environ. Int. 127, 785-800.

Alfaro, M. R., Araújo doNascimento, C. W., Miranda Biondi, C., da Silva, Y. J. A. B., de AguiarAccioly, A. M., Montero, A., Ugarte, O. M. and Esteveze, J. (2018) Rare-earth-element geochemistry in soils developed in different geological settings of Cuba. Catena 162, 317-324.

Banks, D., Hall, G., Reimanna, C. and Siewers, U. (1999). Distribution of rare earth elements in crystalline bedrock groundwaters: Oslo and Bergen regions, Norway. Appl. Geochem. 14, 27-39.

Bau, M. and Koschinsky, A. (2009) Oxidative scavenging of cerium on hydrous Fe oxide: Evidence from the distribution of rare earth elements and yttrium between Fe oxides and Mn oxides in hydrogenetic ferromanganese crusts. Geochem. J. 43, 37-47.

Blatt, H., Middleton, G. V. and Murray, R. C. (1980) Origin of Sedimentary Rocks (2nd edition). New Jersey: Prentice-Hall, 1-634.

Chen, W. H. and Ni, M. Y. (1987) Quaternary Geology in Hebei. Geological Publish House, Beijing, China. (In Chinese).

Chen, W. H. (1999) Groundwater in Hebei. Seismological Press, Beijing, (In Chinese).

Chen, Z. Y., Nie, Z. L., Zhang, Z. J., Qi, J. X., Nan, Y. J. (2005) Isotopes and sustainability of ground water resources, North China Plain. Groundwater, 43, 485-493.

Cheng, H., Hao, F., Ouyang, W., Liu, S., Lin, C.Y. and Yang, W. (2012) Vertical distribution of rare earth elements in a wetland soil core from the Sanjiang Plain in China. J. Rare Earth 30, 731-738.

Compton, J. S., White, R. A. and Smith, M. (2003) Rare earth element behavior in soils and salt pan sediments of a semi-arid granitic terrain in the Western Cape, South Africa. Chem. Geol. 201 (3-4), 239-255.

Consani, S., Cutroneo, L., Carbone, C. and Capello, M. (2020) Baseline of distribution and origin of Rare Earth Elements in marine sediment of the coastal area of the Eastern Gulf of Tigullio (Ligurian Sea, North-West Italy). Mar. Pollut. Bull. 155, 111145.

Cox, R., Lowe, D. R. and Cullers, R. L. (1995) The influence of sediment recycling and basement composition on evolution of mudrock chemistry in the southwestern United States. Geochim. Cosmochim. Acta 59(14), 2919-29440.

Davranche, M., Grybos, M., Gruau, G., Pédrot, M., Dia, A. and Marsac, R. (2011) Rare earth element patterns: a tool for identifying trace metal sources during wetland soil reduction. Chem. Geol. 284(1-2), 0-137.

Dostal, J. and Keppie, J. D. (2009) Geochemistry of low-grade ctastic rocks in the Acatl An Complex of southern Mexico: Evidence for local provenance in felsie-intermediate igneous rocks. Sediment. Geol. 222(3-4), 241-253.

509 Ebrahimi, P. and Barbieri, M. (2019) Gadolinium as an emerging microcontaminant in
510 water resources: threats and opportunities. Geosciences (Switzerland) 9(2), 93.
511 Fedo, C. M., Nesbitt, H. W., Young and G. M. (1995) Unraveling the effects of
512 potassium metasomatism in sedimentary rocks and paleosols with implications
513 for paleoweathering conditions and provenance. Geology 23, 921-924.
514 GB/T 14506. (2010). Methods for chemical analysis of silicate rocks.
515 Guo, H. M., Zhang, B., Wang, G. C. and Shen, Z. L. (2010) Geochemical controls on
516 arsenic and rare earth elements approximately along a groundwater flow path in
517 the shallow aquifer of the Hetao Basin, Inner Mongolia. Chem. Geol. 270,
518 117-125.
519 Han, G. L., Song, Z. L. and Tang, Y. (2017) Geochemistry of rare earth elements in
520 soils under different land uses in a typical karst area, Guizhou Province,
521 Southwest China. Can. J. Soil Sci. 97, 606-612.
522 Hatje, V., Bruland, K. W. and Flegal, A. R. (2016) Increases in anthropogenic
523 gadolinium anomalies and rare earth element concentrations in San Francisco
524 Bay over a twenty-year record. Environ. Sci. Technol. 50, 4159-4168.
525 Henderson, P. (1984) Rare earth element geochemistry, Elsevier, Amsterdam.
526 Hu, Z., Richter, H., Sparovek, G. and Schnug, E. (2004) Physiological and
527 biochemical effects of rare earth elements on plants and their agricultural
528 significance: a review. J. Plant Nutr. 27, 183-220.
529 Hu, Z. Y., Haneklaus, S., Sparovek, G. and Schnug, E. (2006) Rare earth elements in
530 soils. Commun. Soil Sci. Plant 37(9-10), 1381-1420.

Kendy, E., Zhang, Y., Liu, C., Wang, J. and Steenhuis, T. (2004) Groundwater recharge from irrigated cropland in the North China Plain: case study of Luancheng County, Hebei Province, 1949-2000. Hydrol. Process. 18(12), 2289-2302.

Kimoto, A., Nearing, M. A., Zhang, X. C. and Powell, D. M. (2006) Applicability of rare earth element oxides as a sediment tracer for coarse-textured soils. Catena 65 (3), 214-221.

Kulaksız, S. and Bau, M. (2013) Anthropogenic dissolved and colloid/nanoparticle-bound samarium, lanthanum and gadolinium in the Rhine River and the impending destruction of the natural rare earth element distribution in rivers. Earth Planet Sc. Lett. 362, 43-50.

LaMaskin, T. A., Dorsey, R. J. and Vervoort, J. D. (2008) Tectonic controls on mudrock geochemistry Mesozoic rocks of eastern Oregon and western Idaho. U.S.A.:Implications for Cordilleran tectonics. J. Sediment. Res. 78(12), 765-783.

Lan, X. H., Li, R. H., Mi, B. B., Zhang, Z. X., Guo, X. W. and Long, H. (2016) Distribution characteristics of rare earth elements in surface sediment and their provenance discrimination in the eastern Bohai and northern Yellow Seas. Earth Sci. 41(3), 462. (In Chinese with English abstract).

Laveuf, C. and Cornu, S. (2009) A review on the potentiality of rare earth elements to trace pedogenetic processes. Geoderma 154, 1-12.

Lee, S. G., Lee, D. H., Kim, Y., Chae, B. G., Kim, W. Y. and Woo, N. C. (2003) Rare earth elements as indicators of groundwater environment changes in a fractured

553 rock system: evidence from fracture-filling calcite. Appl. Geochem. 18, 135-143.
554 Li, J., Hong, M., Yin, X. and Liu, J. (2010) Effects of the accumulation of the rare
555 earth elements on soil macrofauna community. J. Rare Earth 28, 957-964.
556 Liang, T., Zhang, S., Wang, L. J., Kung, H. T., Wang, Y. Q., Hu, A. T. and Ding, S. M.,
557 (2005) Environmental biogeochemical behaviors of rare earth elements in
558 soil-plant systems. Environ. Geochem. Health 27, 301-311.
559 Lin, C. Y., Liu, S. Q., He, M. C. and Li, R. P. (2013) Distribution of rare earth
560 elements in the estuarine and coastal sediments of the daliao river system, China.
561 J. Radioanal. Nucl. Ch. 298(1), 627-634.
562 Liu, H. Y., Guo, H. M., Xing, L. N., Zhan, Y. H., Li, F. L., Shao, J. L., N, H., L, X.
563 and Li, C.Q. (2016) Geochemical behaviors of rare earth elements in
564 groundwater along a flow path in the North China Plain. J. Asian Earth Sci. 117,
565 33-51.
566 Liu, H. Y, Pourret, O., Guo, H. M. and Bonhoure, J. (2017) Rare earth elements
567 sorption to iron oxyhydroxide: Model development and application to
568 groundwater. Appl. Geochem. 87, 158-166.
569 Liu, H. Y., Guo, H. M., Pourret O., Chen, Y. and Yuan, R. X. (2019a) Role of
570 manganese oxyhydroxides in the transport of rare earth elements along a
571 groundwater flow path. Int. J. Environ. Res. Public Health 16, 2263.
572 Liu, J., Song, J. M., Yuan, H. M., Li, X. G., Li, N. and Duan, L. Q. (2019b) Rare earth
573 element and yttrium geochemistry in sinking particles and sediments of the
574 Jiaozhou Bay, North China: Potential proxy assessment for sediment

resuspension. Mar. Pollut. Bull. 144, 79-91.

McLennan, S. M. (1989) Rare earth elements in sedimentary rocks: Influence of provenance and sedimentary processes. Rev. Mineral. Geochem. 21, 169-200.

McLennan, S. M. (2001) Relationships between the trace element composition of sedimentary rocks and upper continental crust. Geochemistry, Geophysics, Geosystems, 2(4).

Mihajlovic, J. and Rinklebe, J. (2018) Rare earth elements in German soils-A review. Chemosphere 205(AUG), 514-523.

Mihajlovic, J., Bauriegel, A., Stärk, H. J., Roßkopf, N., Zeitz, J., Milbert, G. and Rinklebe, J. (2019) Rare earth elements in soil profiles of various ecosystems across Germany. Appl. Geochem. 102, 197-217.

Moffett, J. W. (1990) Microbially mediated cerium oxidation in seawater. Nature 345, 421-423.

Nesbitt, H. W., Markovics, G. and Price, R. C. (1980) Chemical processes affecting alkalis and alkaline earths during continental weathering. Geochim. Cosmochim. Acta 44 (11), 1659-1666.

Nesbitt, H. W. and Young, G. M. (1982) Early Proterozoic climates and plate motions inferred from major chemistry of lutites. Nature, 299, 19-40.

Ohta, A. and Kawabe, I. (2000) Rare earth element partitioning between Fe oxyhydroxide precipitates and aqueous NaCl solutions doped with $NaHCO_3$: Determinations of rare earth element complexation constants with carbonate ions. Geochem. J. 34, 439-454.

597 Oliveira, S. M. B., Larizzatti, F. E., Fávaro, D. I. T., Moreira, S. R. D., Mazzilli, B. P.
598 and Piovano, E. L. (2003) Rare earth element patterns in lake sediments as
599 studied by neutron activation analysis. J. Radioanal. Nucl. Ch. 258, 531-535.
600 Panahi, A., Young, G. M and Rainbird, R. H. (2000) Behavior of major and trace
601 elements (including REE) during Paleoproterozoic pedogenesis and diagenetic
602 alteration of an Arehean granite near Ville Marie, Québee, Canada. Geochim.
603 Cosmochim. Acta 64(13), 2199-2220.
604 Pang, X., Li, D. and Peng, A. (2002) Application of rare-earth elements in the
605 agriculture of China and its environmental behavior in soil. Environ. Sci. Pollut.
606 Res. 9, 143-148.
607 Pourret, O. and Davranche, M. (2013) Rare earth element sorption onto hydrous
608 manganese oxide: A modeling study. J. Colloid Interf. Sci. 395, 18-23.
609 Pourret, O. and Tuduri, J. (2017) Continental shelves as potential resource of rare
610 earth elements. Sci. Rep. 7, 585.
611 Pédrot, M., Dia, A., Davranche, M. and Gruau, G. (2015) Upper soil horizons control
612 the rare earth element patterns in shallow groundwater. Geoderma, 239-240,
613 84-96.
614 Sá Paye, H., de, Mello, J. W. V., de, Magalhães Mascarenhas, G. R. L., de and
615 Gasparon, M. (2016) Distribution and fractionation of the rare earth elements in
616 Brazilian soils. J. Geochem. Explor. 161, 27-41.
617 Shao, S. X., Guo, S. Q. and Han, S. H. (1989) Geomorphical structures and evolution
618 of the Huanghuaihai plain in China. Acta Geosicien. Sin. 44(3), 314-322.

619 Silva, Y. J. A. B., Cantalice, J. R. B., Singh, V. P., Nascimento, C. W. A., Piscoya, V. C.
620 and Guerra, S. M. S. (2015) Trace element fluxes in sediments of an
621 environmentally impacted. Environ. Sci. Pollut. Res. 22, 14755-14766.
622 Steinmann, M. and Stille, P. (2008) Controls on transport and fractionation of the rare
623 earth elements in stream water of a mixed basaltic-granitic catchment basin
624 (Massif Central, France). Chem. Geol. 254(1), 1-18.
625 Šmuc, N. R., Dolenec, T., Serafimovski, T., Dolenec, M. and Vrhovnik, P. (2012)
626 Geochemical characteristics of rare earth elements (REEs) in the paddy soil and
627 rice (Oryza sativa L.) system of Kočani Field, Republic of Macedonia.
628 Geoderma, 183-184, 1-11.
629 Tanaka, K., Tani, Y., Takahashi, Y., Tanimizu, M., Suzuki, Y., Kozai, N. and Ohnuki, T.
630 (2010) A specific Ce oxidation process during sorption of rare earth elements on
631 biogenic Mn oxide produced by Acremonium sp. Strain KR21-2. Geochim.
632 Cosmochim. Acta 74, 5463-5477.
633 Taylor, S. R. and McLennan, S. M. (1985) The Continental Crust: Its Composition
634 and Evolution. Blackwell, Boston, 312 pp.
635 Tyler, G. (2004) Rare earth elements in soil and plant systems-a review. Plant and Soil.
636 267 (1-2), 191-206.
637 Verplanck, P. P., Taylor, H. E., Nordstrom, D. K. and Barber, L. B. (2005) Aqueous
638 Stability of Gadolinium in Surface Waters Receiving Sewage Treatment Plant
639 Effluent, Boulder Creek, Colorado. Environ. Sci. Technol. 39 (18), 6923-6929.
640 Wang, S. H., Zhang, N., Chen, H., Li, L., Yan, W. (2014) The surface sediment type

641 and their rare earth element characteristics from the continental shelf of the
642 northern South China Sea. Cont. Shelf Res. 88, 185-202.
643 Wang, L. and Liang, T. (2015) Geochemical fractions of rare earth elements in soil
644 around a mine tailing in Baotou, China. Sci. Rep. 5, 12483.
645 Wang, L., Han, X., Liang, T., Guo, Q., Li, J., Dai, L. and Ding, S. (2018)
646 Discrimination of rare earth element geochemistry and co-occurrence in
647 sediment from Poyang Lake, the largest freshwater lake in China. Chemosphere
648 217, 851-857.
649 Wei, L., Guo, H. M., Xie, Z. H. and Li, Z. P. (2010) Rare earth elements geochemistry
650 and its implication for sediment provenance in the Beijing plain, Earth Sci. Front.
651 17(6), 72-80. (In Chinese with English abstract).
652 Wei, F. S., Liu, T. L., Teng, E. J. and Rui, K. S. (1991) A survey on the background
653 contents of 15 rare earth elements in Chinese soil. Environ. Sci. 12, 78-82 (In
654 Chinese with English abstract).
655 Wu, J., Lu, J., Li, L. M., Min, X. Y., Zhang, Z. H. and Luo Y. M. (2018) Distribution,
656 pollution, and ecological risks of rare earth elements in soil of the northeastern
657 Qinghai-tibet plateau. Hum. Ecol. Risk Assess. 25(3), 1-16.
658 Xie, X. J., Wang, Y. X., Ellis, A., Liu, C. X., Duan, M. Y. and Li, J. X. (2014) Impact
659 of sedimentary provenance and weathering on arsenic distribution in aquifers of
660 the Datong basin, China: Constraints from elemental geochemistry. J. Hydrol.
661 519, 3541-3549.
662 Xing, L. N., Guo, H. M. and Zhan, Y. H. (2013) Groundwater hydrochemical

characteristics and processes along flow paths in the North China Plain. J. Asian Earth Sci. 70-71, 250-264.

Xu, N., Morgan, B. and W. Rate, A. (2018) From source to sink: Rare-earth elements trace the legacy of sulfuric dredge spoils on estuarine sediments. Sci. Total Environ. 637-638, 1537-1549.

Yan, X. P., Kerrich, R. and Hendry, M. J. (1999) Sequential leachates of multiple grain size fractions from a clay-rich till, Saskatchewan, Canada: implications for controls on the rare earth element geochemistry of porewaters in an aquitard. Chem. Geol. 158, 53-79.

Yang, S. Y., Jung, H. S., Choi, M. S. and Li, C. X. (2002) The rare earth element compositions of the Changjiang (Yangtze) and Huanghe (Yellow) river sediments. Earth Planet Sc. Lett. 201, 407-419.

Yu, C., Drake, H., Mathurin, F. A. and Åström, M. E. (2017) Cerium sequestration and accumulation in fractured crystalline bedrock: The role of Mn-Fe (hydr-) oxides and clay minerals. Geochim. Cosmochim. Acta 199, 370-389.

Zhang, R. Q., Liang, X., Jing, M. M., Wan, L. and Yu, Q. C. (2018) Fundamental of hydrogeology, 7th edition, Geological Publishing House, Beijing, 121-123. (In Chinese).

Zhang, Y. and Gao, X. L. (2015) Rare earth elements in surface sediments of a marine coast under heavy anthropogenic influence: The Bohai Bay, China. Estuar. Coastal Shelf S. 164, 86-93.

Figure and Table captions

Table 1 Concentrations of REE and major oxides and REE fractionation indices in the sediment samples from three zones

Table 2 Pearson's correlations between REE concentrations and major oxides, CIA and LOI in the sediment samples from three zones (Y09 (118 m): piedmont, n = 50; S30 (184 m): central, n=163; H02 (110 m): littoral, n = 63; "**" indicates $p < 0.01$, "*" $p < 0.05$)

Figure 1 Study area and sediments sampling locations (boreholes)

Figure 2 Changes of sediment lithology and REE parameters along depth: (a) piedmont borehole Y09, (b) central borehole S30, (c) littoral borehole H02.

Figure 3 Ternary diagram of sandstone classification and Al_2O_3-CaO+Na_2O-K_2O (A-CN-K)

Figure 4 NASC normalized REE patterns and absolute REE concentrations all sediment samples (The line indicates a trend of normalized REE concentrations. The box-whisker shows distributions of absolute REE concentrations)

Figure 5 Total REE concentrations as a function of $(La/Yb)_{NASC}$ (a), Ce/Ce* (c) and Eu/Eu* (d); a relationship between CIA and $(La/Yb)_{NASC}$ (b).

707

708 Table 1

Component	Unit	piedmont Y09			central S30			littoral H02		
		Min.	Avg.	Max.	Min.	Avg.	Max.	Min.	Avg.	Max.
La	mg/kg	19.54	40.93	63.81	16.59	33.16	54.53	16.80	32.05	43.99
Ce	mg/kg	39.75	82.99	135.94	31.99	66.34	108.59	31.81	63.09	87.26
Pr	mg/kg	4.60	9.71	14.98	3.87	7.72	12.38	3.87	7.39	10.01
Nd	mg/kg	16.50	35.71	55.46	13.96	28.41	45.28	13.70	27.28	36.75
Sm	mg/kg	3.12	6.81	10.43	2.66	5.56	8.73	2.58	5.40	7.30
Eu	mg/kg	0.70	1.31	1.91	0.72	1.12	1.60	0.72	1.09	1.50
Gd	mg/kg	2.73	6.09	9.67	2.32	4.99	7.72	2.22	4.87	6.97
Tb	mg/kg	0.45	0.97	1.52	0.34	0.78	1.24	0.34	0.78	1.10
Dy	mg/kg	2.49	5.41	8.35	1.97	4.34	6.75	1.97	4.32	6.03
Ho	mg/kg	0.55	1.11	1.70	0.40	0.88	1.35	0.41	0.88	1.22
Er	mg/kg	1.53	3.10	4.42	1.11	2.46	3.72	1.08	2.47	3.40
Tm	mg/kg	0.26	0.53	0.75	0.19	0.42	0.64	0.20	0.43	0.59
Yb	mg/kg	1.59	3.20	4.47	1.24	2.64	3.93	1.18	2.62	3.50
Lu	mg/kg	0.27	0.53	0.73	0.20	0.44	0.66	0.21	0.44	0.60
Y	mg/kg	14.60	30.20	44.94	10.53	23.61	36.11	10.80	23.59	34.05
SiO_2	wt%	55.55	66.77	78.36	35.71	56.62	71.56	32.04	59.51	77.03
Fe_2O_3	wt%	1.86	5.46	9.86	2.00	4.45	6.51	1.83	4.06	6.61
Al_2O_3	wt%	6.37	10.47	14.14	7.42	10.95	13.82	7.32	12.18	15.96
MgO	wt%	0.27	1.38	2.41	1.01	2.34	3.70	0.61	2.14	5.27
CaO	wt%	0.40	1.25	5.45	0.97	7.01	19.23	1.30	6.12	18.63
Na_2O	wt%	0.15	1.15	2.28	0.66	1.65	3.31	0.52	3.38	46.29
K_2O	wt%	1.89	2.58	3.37	1.55	2.20	2.82	1.57	2.26	2.89
MnO	wt%	0.02	0.07	0.30	0.03	0.07	0.15	0.04	0.07	0.16
P_2O_5	wt%	0.06	0.1	0.69	0.13	0.25	0.36	0.04	0.12	0.17
TiO_2	wt%	0.26	0.69	0.99	0.44	0.93	1.54	0.51	0.96	1.22
LOI	wt%	1.13	3.88	7.36	3.12	8.56	19.91	2.5	8.02	17.56
∑REE	mg/kg	109	229	354	89	183	291	88	177	238
LREE	mg/kg	84	178	279	70	142	231	7	136	183
HREE	mg/kg	9.93	20.94	31.59	7.77	16.96	26.00	7.61	16.81	23.39
LREE/HREE	-	6.93	8.43	10.83	7.51	8.36	9.69	7.33	8.15	9.80
Ce/Ce*	-	0.69	0.91	1.17	0.85	0.90	0.98	0.80	0.89	0.98
Eu/Eu*	-	0.82	0.91	1.07	0.83	0.95	1.31	0.86	0.95	1.34
Gd/Gd*	-	0.95	1.06	1.15	0.93	1.05	1.12	0.87	1.04	1.10
$(Y/Ho)_{NASC}$	-	1.09	1.13	1.22	1.04	1.11	1.17	1.06	1.11	1.19
$(La/Yb)_{NASC}$	-	0.86	1.23	1.15	1.03	1.21	1.49	0.91	1.09	1.49

709

710 **Table 2**

	borehole	REE	SiO_2	Fe_2O_3	Al_2O_3	MgO	CaO	Na_2O	K_2O	LOI	CIA
REE	Y09	1									
	S30	1									
	H02	1									
SiO_2	Y09	-0.79**	1								
	S30	-0.58**	1								
	H02	-0.67**	1								
Fe_2O_3	Y09	0.72**	-0.92**	1							
	S30	0.90**	-0.56**	1							
	H02	0.89**	-0.67**	1							
Al_2O_3	Y09	0.67**	-0.77**	0.85**	1						
	S30	0.51**	0.249**	0.60**	1						
	H02	0.19	0.430**	0.30*	1						
MgO	Y09	0.55**	-0.77**	0.79**	0.55**	1					
	S30	0.66**	-0.61**	0.79**	0.31**	1					
	H02	0.71**	-0.84**	0.71**	-0.32**	1					
CaO	Y09	-0.06	-0.11	0.05	-0.342*	0.44**	1				
	S30	0.12	-0.82**	0.04	-0.72**	0.21*	1				
	H02	0.15	-0.58**	0.06	-0.40**	0.12	1				
Na_2O	Y09	-0.74**	0.78**	-0.70**	-0.79**	-0.31*	0.31*	1			

	S30	-0.81**	0.79**	-0.75**	-0.24*	-0.57**	-0.44**	1			
	H02	0.19	-0.51**	0.13	-0.76**	0.68**	-0.07	1			
	Y09	0.13	-0.09	0.001	-0.125	-0.19	-0.40**	-0.18	1		
K_2O	S30	0.17	0.26**	0.36**	0.58**	0.17	-0.61**	0.09	1		
	H02	0.17	-0.003	0.46**	0.49**	0.08	-0.39**	-0.19	1		
	Y09	0.50**	-0.84**	0.60**	0.46**	0.44**	0.03	-0.52**	-0.003	1	
LOI	S30	0.21*	0.91**	0.16	0.64**	0.23*	0.83**	0.52**	1.74	1	
	H02	0.27*	0.85**	0.25*	0.47**	0.42**	0.62**	-0.04	-0.03	1	
	Y09	0.51**	-0.75**	0.82**	0.54**	0.44**	-0.003	-0.66**	-0.04**	0.56**	1
CIA	S30	0.26	0.06	0.36**	0.02	0.09	-0.52**	-0.06	0.34**	0.002	1
	H02	0.35**	0.03	0.48**	0.25*	0.26*	-0.29*	-0.01	0.21*	-0.01	1

711

712

713

714

715

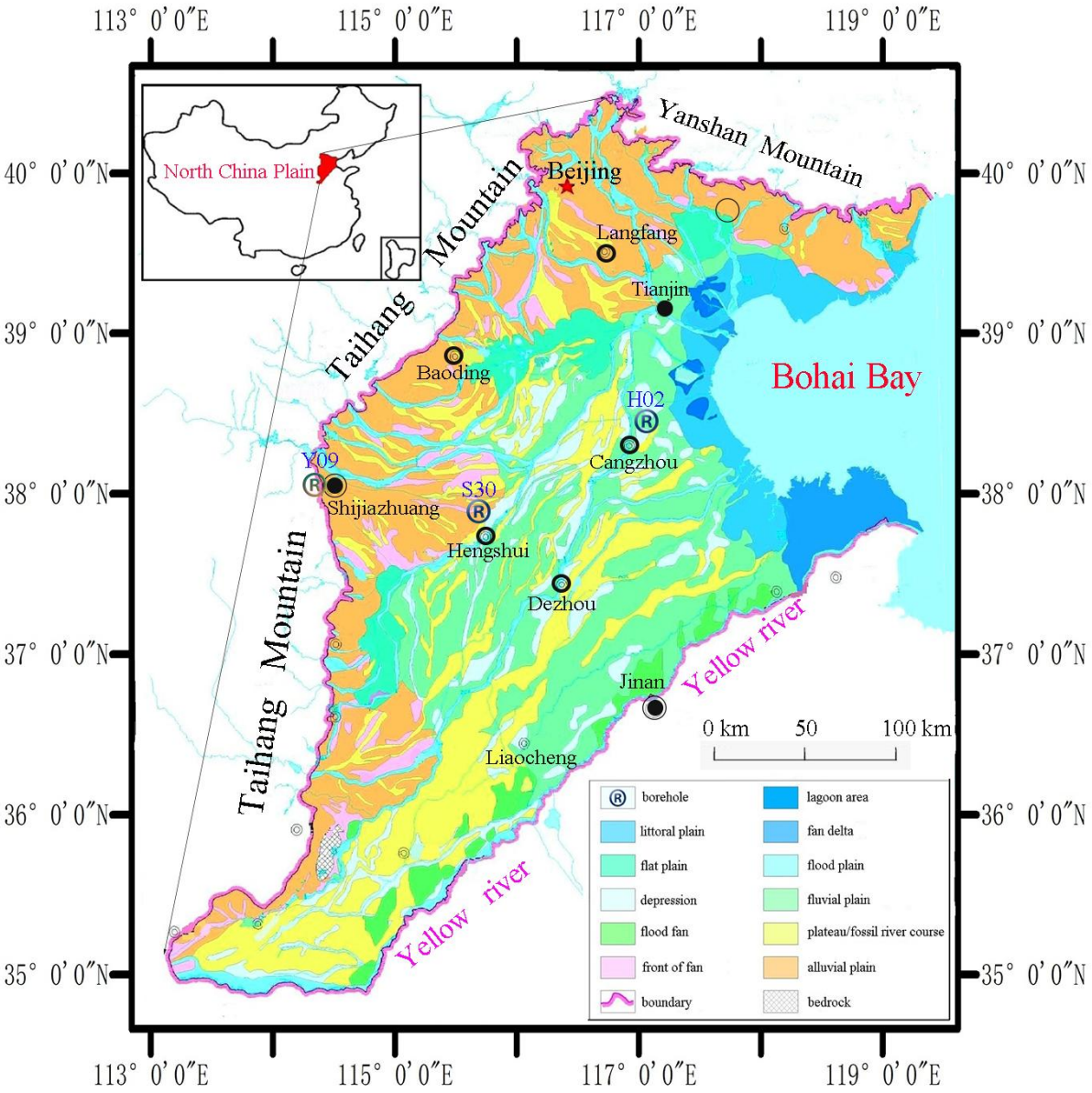

716
717
718 **Fig. 1**
719
720
721
722

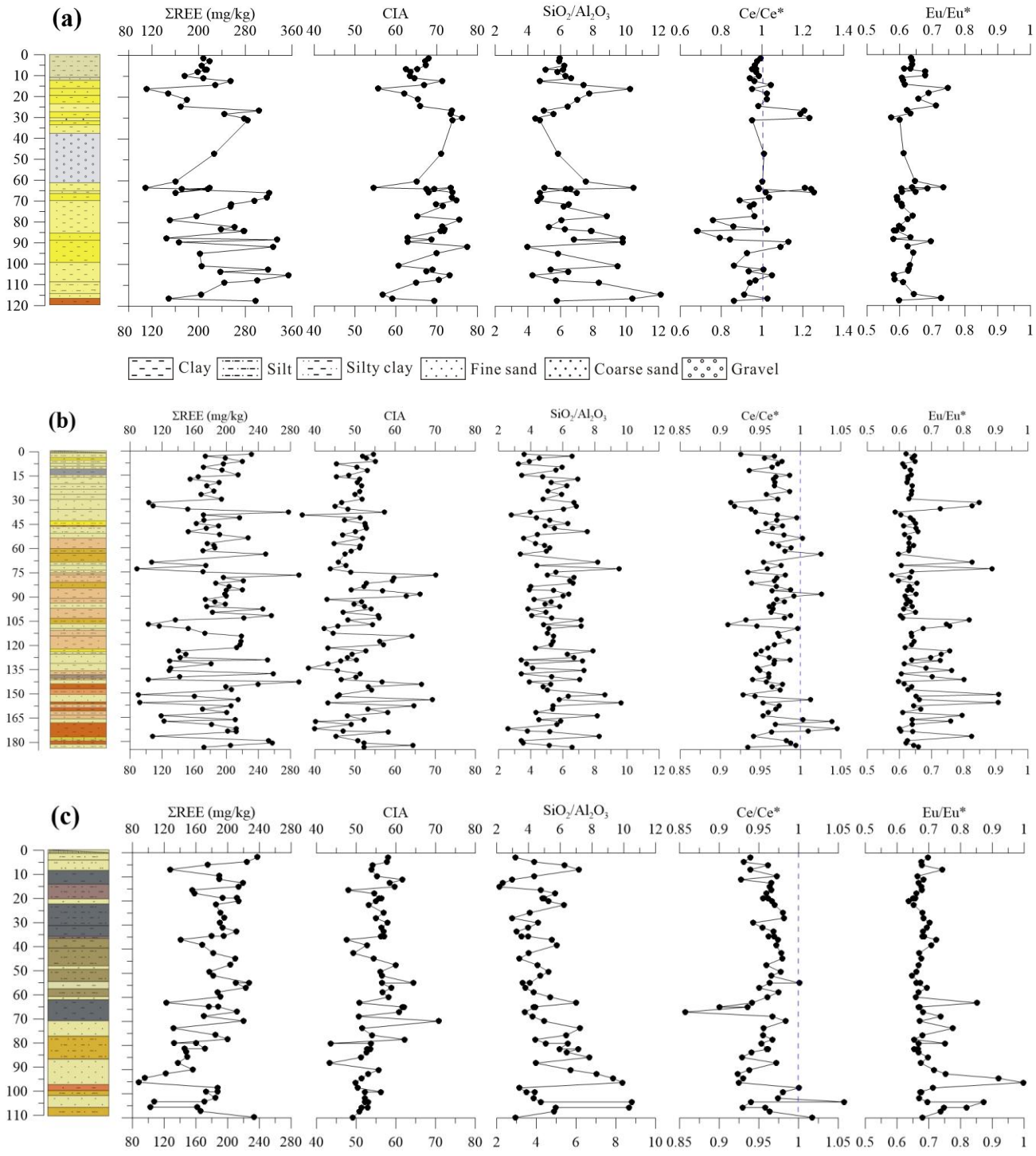

723

724

725

726 **Fig. 2**

727

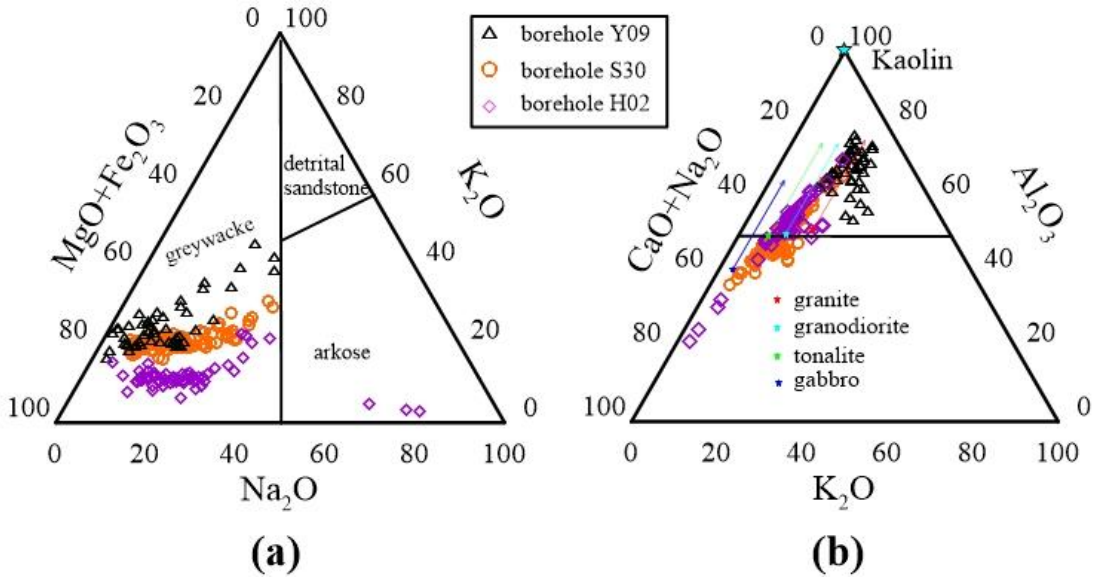
borehole Y09
borehole S30
borehole H02
detrital sandstone
greywacke
arkose
MgO+Fe2O3
K2O
Na2O
(a)
Kaolin
CaO+Na2O
Al2O3
granite
granodiorite
tonalite
gabbro
K2O
(b)

Fig. 3

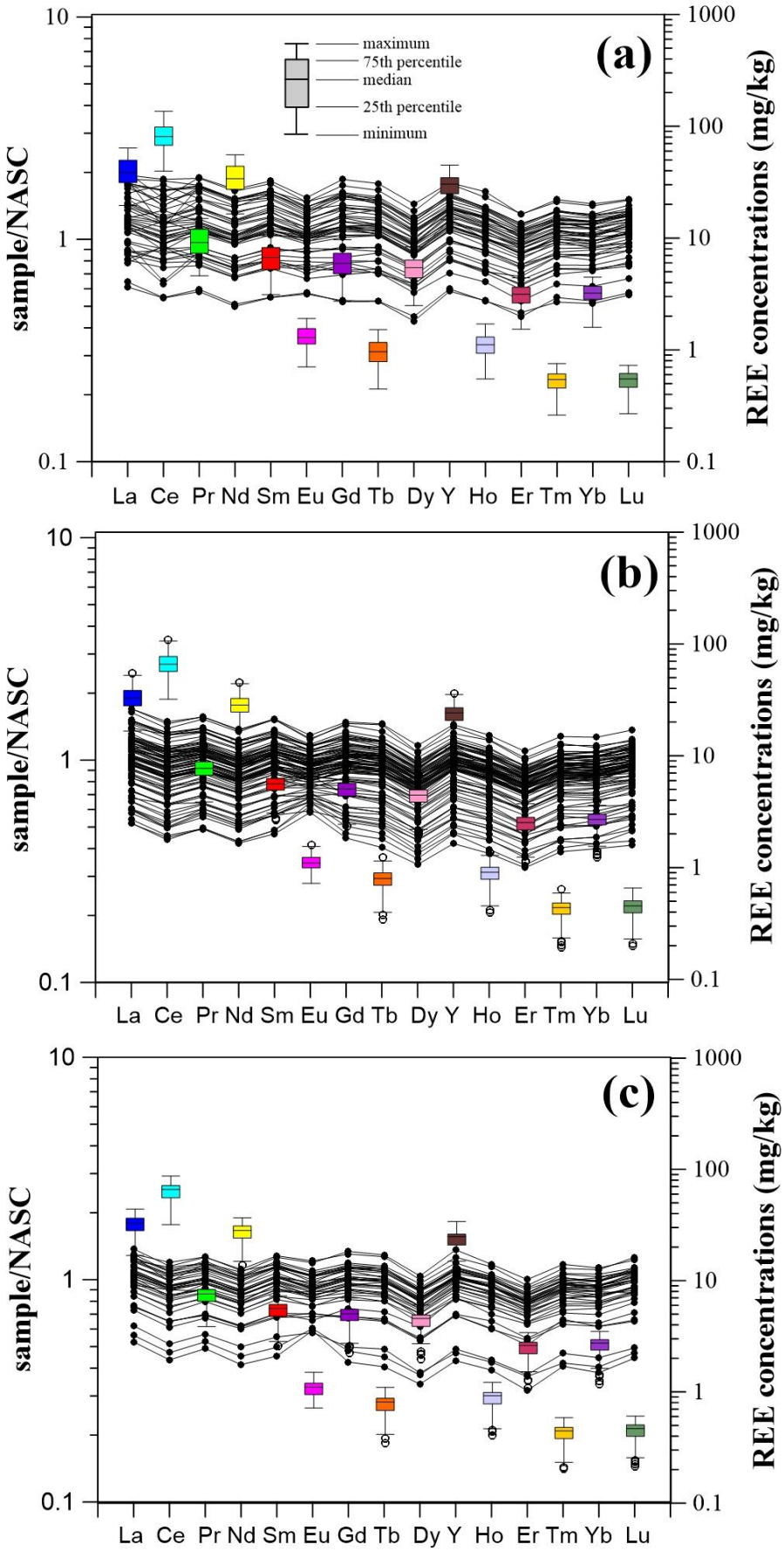
(a)
maximum
75th percentile
median
25th percentile
minimum
sample/NASC
REE concentrations (mg/kg)
10
1
0.1
1000
100
10
1
0.1
La Ce Pr Nd Sm Eu Gd Tb Dy Y Ho Er Tm Yb Lu
(b)
sample/NASC
REE concentrations (mg/kg)
La Ce Pr Nd Sm Eu Gd Tb Dy Y Ho Er Tm Yb Lu
(c)
sample/NASC
REE concentrations (mg/kg)
La Ce Pr Nd Sm Eu Gd Tb Dy Y Ho Er Tm Yb Lu

736

737 **Fig. 4**

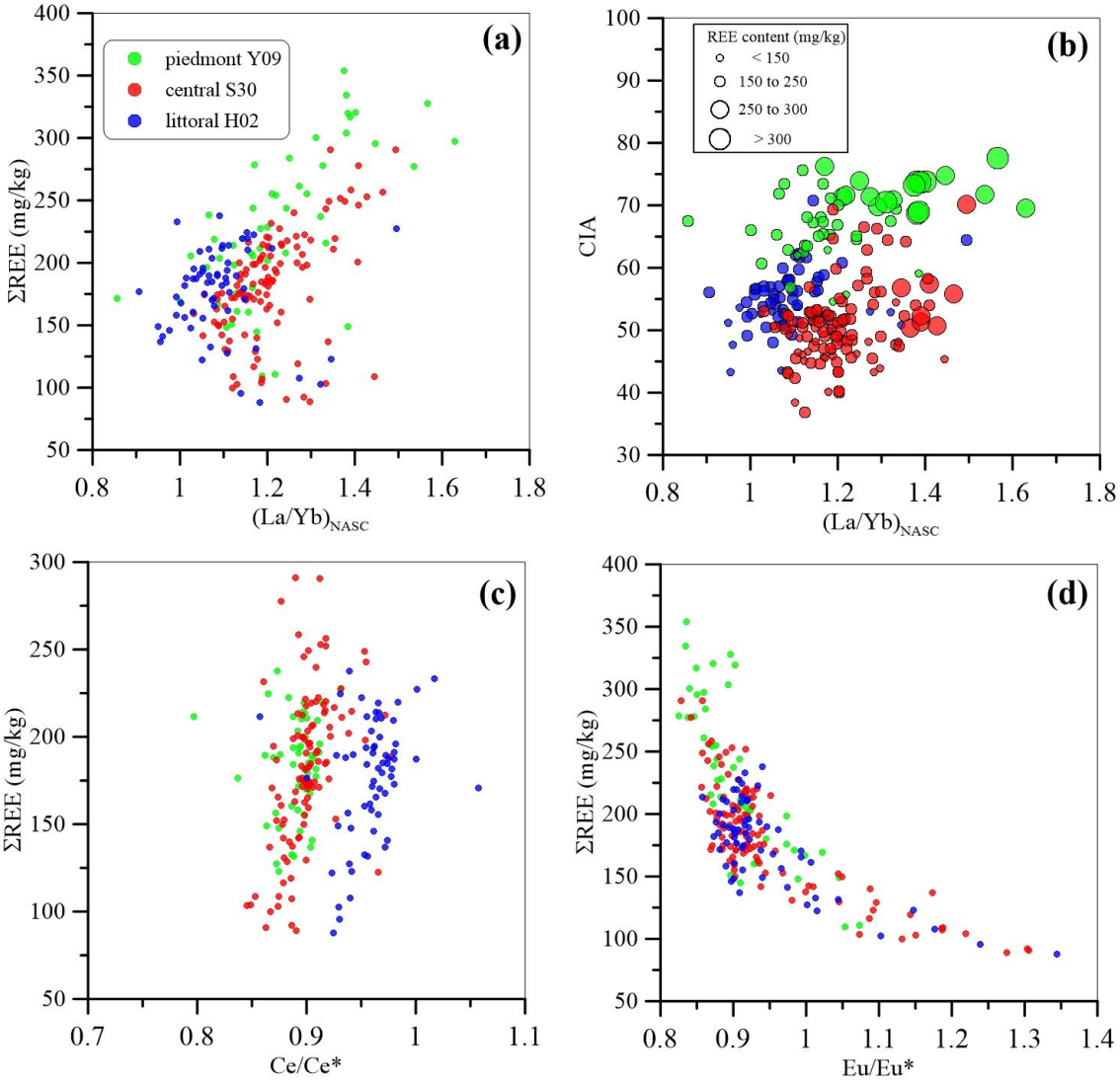
(a)
piedmont Y09
central S30
littoral H02
ΣREE (mg/kg)
(La/Yb)NASC
(b)
REE content (mg/kg)
< 150
150 to 250
250 to 300
> 300
CIA
(La/Yb)NASC
(c)
ΣREE (mg/kg)
Ce/Ce*
(d)
ΣREE (mg/kg)
Eu/Eu*

Fig. 5